2023-03-10

The nonlinear BenjaminFeir instability Hamiltonian dynamics, discrete breathers and steady solutions

Andrade, D

10.1017/jfm.2023.96
Journal of Fluid Mechanics
Cambridge University Press (CUP)

J. Fluid Mech. (2023), *vol*. 958, A17, doi:10.1017/jfm.2023.96

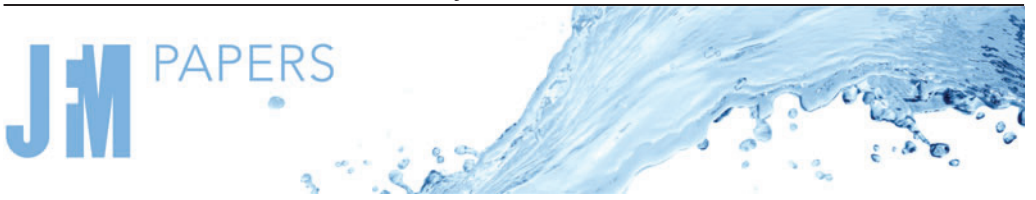

The nonlinear Benjamin–Feir instability – Hamiltonian dynamics, discrete breathers and steady solutions

David Andrade[1,2] **and Raphael Stuhlmeier**[1,†]

[1]Centre for Mathematical Sciences, University of Plymouth, Drake Circus, PL4 8AA Plymouth, UK

[2]School of Engineering, Science and Technology, Universidad del Rosario, 111711 Bogotá, Colombia

(Received 23 August 2022; revised 25 January 2023; accepted 26 January 2023)

We develop a general framework to describe the cubically nonlinear interaction of a degenerate quartet of deep-water gravity waves in one or two spatial dimensions. Starting from the discretised Zakharov equation, and thus without restriction on spectral bandwidth, we derive a planar Hamiltonian system in terms of the dynamic phase and a modal amplitude. This is characterised by two free parameters: the wave action and the mode separation between the carrier and the sidebands. For unidirectional waves, the mode separation serves as a bifurcation parameter, which allows us to fully classify the dynamics. Centres of our system correspond to non-trivial, steady-state nearly resonant degenerate quartets. The existence of saddle-points is connected to the instability of uniform and bichromatic wave trains, generalising the classical picture of the Benjamin–Feir instability. Moreover, heteroclinic orbits are found to correspond to discrete, three-mode breather solutions, including an analogue of the famed Akhmediev breather solution of the nonlinear Schrödinger equation.

Key words: surface gravity waves

1. Introduction

The linear theory of water waves, developed and refined over the course of the 19th and early 20th centuries, has endured by virtue of its simplicity, elegance and utility. When the governing equations are linearised, waves may be superposed to create the myriad complex patterns observed on the surface of the sea. The absence of interaction among

† Email address for correspondence: raphael.stuhlmeier@plymouth.ac.uk

such waves leads, however, to an inability to explain certain properties of ocean wave fields, particularly if these waves are steep or the time scales considered are long.

This interaction may occur between a wave and itself, as discovered by Stokes (1847), or as a mutual interaction between different waves. A natural way to think about such weakly nonlinear interactions is as occurring between Fourier modes, each of which represents a periodic wave train (or plane wave) with a distinct frequency, amplitude and phase. When considering gravity waves in deep water, the fundamental interaction is between four such Fourier modes, which may or may not be distinct. This fact is not obvious *a priori*, as it depends on the possibility of resonance between modes and therefore on the dispersion relation of the problem. The deep-water dispersion relation $\omega^2 = g|\boldsymbol{k}|$ between radian frequency ω and wavenumber vector $\boldsymbol{k}$ provides a geometric constraint which means resonance is possible for cubic (or higher) nonlinearity. This pioneering discovery by Phillips (1960) soon became the object of intense study, with work to elucidate its consequences for everything from wave spectra (Hasselmann 1962) to the evolution of uniform wave trains (so-called Stokes waves) (Benjamin & Feir 1967; Zakharov 1968).

One of the most remarkable early results was the finding that initially uniform wave trains are unstable, and tend to disintegrate into wave groups – known as modulational or Benjamin–Feir instability after Benjamin & Feir (1967). Indeed, uniform wave trains are often difficult to produce experimentally, a fact attributed to this instability. The perturbations required to start the process of disintegration are small-amplitude sidebands or Fourier modes to either side of the plane wave. Interaction between the modes transfers energy to the sidebands, which grow at the expense of the plane wave (or carrier) and distort the pattern on the free surface. Shortly after the discovery of this instability, Zakharov (1968) derived a simplified equation governing the evolution of such unidirectional wave groups from the Hamiltonian formulation of the water wave problem, provided the wave modes are not widely separated in Fourier space. This nonlinear Schrödinger equation (NLS) was then used to recover Benjamin and Feir's criterion, specifying which ranges of sideband wavenumbers and carrier steepness give rise to instability.

The nonlinear Schrödinger equation has also received considerable recent attention in connection with the deterministic and stochastic modelling of extreme waves, large wave crests which appear without warning on the surface of the sea (a recent review of progress is given by Onorato & Suret 2016). The temporally or spatially localised exact solutions of the NLS, called 'breathers', are of particular importance to our understanding of extreme waves. Their recent experimental observation (Chabchoub *et al.* 2014) make them an attractive model to generate extreme waves in the wave flume and shed light on the behaviour of such waves in the ocean. Indeed, each breather is a particular manifestation of the underlying Benjamin–Feir instability for special initial conditions.

The success of the NLS as a simplified model equation naturally engendered interest in its agreement with more general water wave equations. The NLS breather solutions, for example, were found to be quite robust when compared to numerical solutions of the Euler equations by Slunyaev & Shrira (2013), who also gave an overview of previous work in this vein. The Benjamin–Feir stability threshold derived from the NLS has also been re-examined by Crawford *et al.* (1981), who sought to remove the restriction to small mode separation. However, the route to obtaining an instability criterion in their work remained one of linearisation and the derivation of an eigenvalue criterion. The smallness assumptions intrinsic to linear stability analysis mean that it is limited to describing only the initial stages of evolution around particular exact solutions. In this setting, the eigenvalues of the linearised system govern the growth rate of initially

small disturbances, whose subsequent evolution can be captured by numerical simulation. However, a numerical treatment has the potential to obscure fundamental, underlying mechanisms, particularly in cases with many (ostensibly independent) parameters. For example, computing the evolution of a carrier and two sidebands requires the specification of eight parameters: two wavenumbers $\boldsymbol{k}_a, \boldsymbol{k}_b$, (the third is given from the resonance condition $2\boldsymbol{k}_a = \boldsymbol{k}_b + \boldsymbol{k}_c$), three wave slopes $\epsilon_a, \epsilon_b, \epsilon_c$, and three phases θ_a, θ_b and θ_c. We aim to present a unified theory of the cubically nonlinear interaction of three waves in deep water, which generalises the Benjamin–Feir instability. Our starting point, like that of Crawford *et al.* (1981), is the reduced Zakharov equation (ZE), which is free from any restrictions on mode separation. Indeed, the nonlinear Schrödinger equation itself, as well as later generalisations due to Davey & Stewartson (1974) or Dysthe (1979), can all be derived as narrowband limits of the ZE (see Stiassnie 1984; Gramstad & Trulsen 2011). After suitable transformations, the interaction of three wave modes satisfying $2\boldsymbol{k}_a = \boldsymbol{k}_b + \boldsymbol{k}_c$ can be recast as a planar Hamiltonian dynamical system. Phase-plane analysis of this system allows for a complete description of the dynamics for all times and arbitrary initial conditions: these initial conditions are reduced to specifying a single 'dynamic phase' and a parameter specifying the distribution of the wave action among the three modes. The mode-separation distance plays the role of a bifurcation parameter in the problem.

With this simplification, we are able to fully classify the dynamics of such 'degenerate quartets' of unidirectional waves. Fixed points in the phase plane correspond to steady-state near-resonant cases of the sort found by Liao, Xu & Stiassnie (2016), and heteroclinic orbits are seen to correspond to a variety of discrete breather-type solutions. We obtain general instability results for uniform and bichromatic wave trains as criteria for the existence of fixed-points, and show that the well-known results of linear stability analysis can be recovered. In what follows, we first present the reformulation of the discrete Zakharov equation for a degenerate quartet of waves in § 2. In § 3, we classify the fixed points and phase-portraits, using mode separation as a bifurcation parameter. The nonlinear stability of wave trains is considered in § 4, and special, heteroclinic solutions are discussed in § 5. Finally, a discussion of our results is presented in § 6. Appendix A contains some simplified expressions for integral kernels used in computations, while Appendix B discusses the comparison of the Zakharov equation and NLS models.

2. The Zakharov equation for a degenerate quartet of waves

Investigating third-order wave–wave interaction on deep water without a bandwidth restriction means that our starting point will be the reduced Zakharov equation:

$$i\frac{\mathrm{d}B_n}{\mathrm{d}t} = \sum_{p,q,r=1}^{N} T_{npqr}\delta_{np}^{qr}\,\mathrm{e}^{\mathrm{i}\Delta_{npqr}t}B_p^*B_qB_r, \quad n = 1, 2, \ldots, N, \tag{2.1}$$

derived by Zakharov (1968), and in Hamiltonian form by Krasitskii (1994), and here written in a convenient discrete formulation. The physics of the water-wave problem are contained in the rather lengthy kernels $T_{npqr} = T(\boldsymbol{k}_n, \boldsymbol{k}_p, \boldsymbol{k}_q, \boldsymbol{k}_r)$. We use δ_{np}^{qr} to denote a Kronecker delta function:

$$\delta_{np}^{qr} = \begin{cases} 1 & \text{for } \boldsymbol{k}_n + \boldsymbol{k}_p = \boldsymbol{k}_q + \boldsymbol{k}_r \\ 0 & \text{otherwise} \end{cases}, \tag{2.2}$$

and $\Delta_{npqr} = \omega_n + \omega_p - \omega_q - \omega_r$ to denote the frequency detuning (a measure of departure from exact resonance). Throughout,

$$\omega_n^2 = g|\boldsymbol{k}_n| \tag{2.3}$$

is the linear dispersion relation for gravity waves in deep water.

The simplest non-trivial interaction is between three waves in deep water $\boldsymbol{k}_a, \boldsymbol{k}_b$ and $\boldsymbol{k}_c$, where one wave is counted twice to satisfy the resonance condition $2\boldsymbol{k}_a = \boldsymbol{k}_b + \boldsymbol{k}_c$. Indeed this case – termed the 'degenerate quartet' – corresponds to the Benjamin–Feir instability (see Yuen & Lake 1982 or Mei, Stiassnie & Yue 2018, Ch. 14.9), where mode $\boldsymbol{k}_a$ is interpreted as a 'carrier wave' and modes $\boldsymbol{k}_b$ and $\boldsymbol{k}_c$ as 'sidebands'. The resulting system of ordinary differential equations for a degenerate quartet has the same form, albeit with different coefficients, as the one originally derived by Benney (1962).

Rather than handle three complex equations, it is a convenient first step towards simplification to write the discrete equation in terms of amplitude and phase variables (see e.g. Craik (1986) and references therein). The equations then become

$$\frac{\mathrm{d}|B_a|}{\mathrm{d}t} = 2T_{aabc}|B_a||B_b||B_c|\sin(\theta_{aabc}), \tag{2.4a}$$

$$\frac{\mathrm{d}|B_b|}{\mathrm{d}t} = -T_{aabc}|B_a|^2|B_c|\sin(\theta_{aabc}), \tag{2.4b}$$

$$\frac{\mathrm{d}|B_c|}{\mathrm{d}t} = -T_{aabc}|B_a|^2|B_b|\sin(\theta_{aabc}), \tag{2.4c}$$

$$\frac{\mathrm{d}\theta_a}{\mathrm{d}t} = -\Gamma_a - 2\frac{T_{aabc}}{|B_a|^2}|B_a|^2|B_b||B_c|\cos(\theta_{aabc}), \tag{2.4d}$$

$$\frac{\mathrm{d}\theta_b}{\mathrm{d}t} = -\Gamma_b - \frac{T_{aabc}}{|B_b|^2}|B_a|^2|B_b||B_c|\cos(\theta_{aabc}), \tag{2.4e}$$

$$\frac{\mathrm{d}\theta_c}{\mathrm{d}t} = -\Gamma_c - \frac{T_{aabc}}{|B_c|^2}|B_a|^2|B_b||B_c|\cos(\theta_{aabc}), \tag{2.4f}$$

where $\theta_{aabc} = \Delta_{aabc}t - 2\theta_a + \theta_b + \theta_c$ is called the dynamic phase. Note the additional factor of two appearing in the equations for $|B_a|$ and θ_a because the resonance condition $2\boldsymbol{k}_a = \boldsymbol{k}_b + \boldsymbol{k}_c$ can be satisfied for either the tuple $(\boldsymbol{k}_a, \boldsymbol{k}_a, \boldsymbol{k}_b, \boldsymbol{k}_c)$ or $(\boldsymbol{k}_a, \boldsymbol{k}_a, \boldsymbol{k}_c, \boldsymbol{k}_b)$.

In (2.4*d*)–(2.4*f*),

$$\Gamma_i = |B_i|^2 T_i + 2\sum_{j\neq i}|B_j|^2 T_{ij}, \tag{2.5}$$

where we use an abbreviated notation for the symmetric kernels: $T_i = T_{iiii}$, $T_{ij} = T_{ijij} = T_{jiji}$.

The next significant simplification relies on the observation that although there are ostensibly three distinct phases in the equations governing the degenerate quartet (2.4*a*)–(2.4*f*), they occur only in the single combination $2\theta_a - \theta_b - \theta_c$, which makes it possible to drop subscripts and write θ and Δ in place of θ_{aabc} and Δ_{aabc} without risk of confusion. We can further exploit this fact to combine (2.4*d*)–(2.4*f*) into a single equation for the dynamic phase:

$$\frac{\mathrm{d}\theta}{\mathrm{d}t} = \Delta + 2\Gamma_a - \Gamma_b - \Gamma_c + T_{aabc}\left(4|B_b||B_c| - \frac{|B_c||B_a|^2}{|B_b|} - \frac{|B_b||B_a|^2}{|B_c|}\right)\cos(\theta). \tag{2.6}$$

Equations (2.4*a*)–(2.4*c*) and (2.6) now form an autonomous system of ordinary differential equations. It is known that this system of equations admits periodic solutions

which are given in terms of Jacobi elliptic functions, see Shemer & Stiassnie (1985). We shall see that generic solutions are indeed periodic, though we shall focus our attention principally on special, non-periodic solutions. Moreover, we can easily recover the individual phases of the Fourier modes and employ these to reconstruct the leading-order free surface.

The system of (2.4*a*)–(2.4*c*) and (2.6) admits the following conserved quantities:

$$|B_a|^2 + |B_b|^2 + |B_c|^2 = A, \tag{2.7}$$

the total wave action, and

$$\frac{|B_b|^2}{A} - \frac{|B_c|^2}{A} = \alpha, \tag{2.8}$$

the wave-action difference in the two sidebands. These conserved quantities allow us to further reduce the number of parameters by introducing a normalised wave-action variable $\eta = |B_a|^2/A$, which by (2.7), must take values between 0 and 1. The amplitudes may then be rewritten in terms of η and α as $|B_a|^2 = A\eta$, $|B_b|^2 = A(1-\eta+\alpha)/2$ and $|B_c|^2 = A(1-\eta-\alpha)/2$.

In terms of the two variables η and θ, we find that the system can be described by the Hamiltonian:

$$H(\theta,\eta) = -AT_{aabc}2\eta\sqrt{(1-\eta)^2-\alpha^2}\cos(\theta) - (\Delta + A\Omega_0)\eta - \frac{A\Omega_1}{2}\eta^2, \tag{2.9}$$

with

$$\frac{\partial H}{\partial \theta} = \frac{\mathrm{d}\eta}{\mathrm{d}t} = 2AT_{aabc}\eta\sqrt{(1-\eta)^2-\alpha^2}\sin(\theta), \tag{2.10}$$

$$-\frac{\partial H}{\partial \eta} = \frac{\mathrm{d}\theta}{\mathrm{d}t} = \Delta_{aabc} + A\Omega_0 + A\Omega_1\eta + 2AT_{aabc}\frac{1+2\eta^2-3\eta-\alpha^2}{\sqrt{(1-\eta)^2-\alpha^2}}\cos(\theta). \tag{2.11}$$

The two new coefficients are

$$\Omega_0 = 2[T_{ab}(1+\alpha) + T_{ac}(1-\alpha)] - \tfrac{1}{2}[T_b(1+\alpha) + T_c(1-\alpha)] - 2T_{bc}, \tag{2.12}$$

$$\Omega_1 = 2(T_a + T_{bc}) - 4(T_{ab} + T_{ac}) + \tfrac{1}{2}(T_b + T_c). \tag{2.13}$$

Such a Hamiltonian approach to the three-wave discretisation of the nonlinear Schrödinger equation was first explored by Cappellini & Trillo (1991), Trillo & Wabnitz (1991) in the context of optics, and our Hamiltonian (2.9) can be shown to reduce in the narrowband limit to one analogous to that presented therein.

A final simplification of the system can be achieved by imposing an equidistribution of wave action among the sidebands, i.e. $\alpha = 0$. Under this assumption, (2.10) and (2.11), as well as the Hamiltonian (2.9), become

$$\frac{\mathrm{d}\eta}{\mathrm{d}t} = 2AT_{aabc}\eta(1-\eta)\sin(\theta), \tag{2.14}$$

$$\frac{\mathrm{d}\theta}{\mathrm{d}t} = \Delta + A\Omega_0 + A\Omega_1\eta + 2AT_{aabc}(1-2\eta)\cos(\theta), \tag{2.15}$$

$$H(\theta,\eta) = -2AT_{aabc}\eta(1-\eta)\cos(\theta) - (\Delta + A\Omega_0)\eta - \frac{A\Omega_1}{2}\eta^2. \tag{2.16}$$

In subsequent computations, we shall normalise all wavenumbers by the carrier wavenumber k_a, and all frequencies by the carrier frequency ω_a, which is equivalent

to setting the gravitational acceleration $g = 1$. For the unidirectional cases considered, we shall also explicitly specify our degenerate quartets in terms of mode separation p as follows: $\boldsymbol{k}_a = [1, 0]$, $\boldsymbol{k}_b = [1 - p, 0]$ and $\boldsymbol{k}_c = [1 + p, 0]$, where $0 < p < 1$. We henceforth drop the bold-script and write k_i for the wavenumbers, to emphasise that these are scalars. Indeed, for unidirectional waves in deep water, it is possible to significantly simplify the kernels, as shown by Dyachenko, Kachulin & Zakharov (2017), Kachulin, Dyachenko & Gelash (2019) and detailed in Appendix A.

The wave action A of the three-mode system remains a free parameter and the conservation law (2.7) makes it clear that A may be 'distributed' among the three modes in various configurations. The relationship between the complex amplitudes B_i of the Zakharov formulation and the amplitude of the free surface displacement (e.g. (14.5.5) of Mei *et al.* 2018, § 14.5) makes it possible to interpret A in terms of the carrier steepness, which is sometimes convenient. If only the carrier wave is present,

$$A = |B_a|^2 = \frac{2ga^2\pi^2}{\omega_a} = \frac{2\pi^2 g^{1/2}\epsilon^2}{k_a^{5/2}}, \tag{2.17}$$

where a is the surface-wave amplitude and $\epsilon = ak_a$ is the wave slope.

Aside from the wave action A, the system (2.14) and (2.15) contains a further free parameter: the separation between the Fourier modes p. Together, these can be used to determine the values of all coefficients in the equation.

3. Hamiltonian dynamics in the phase plane

The Hamiltonian dynamical system (2.14) and (2.15) describes fully the nonlinear dynamics of three interacting deep-water waves. We can gain both qualitative and quantitative understanding of this system via phase-plane analysis, where the phase space is the surface of the truncated cylinder $\{(\theta, \eta) \mid -\pi \leq \theta \leq \pi, 0 \leq \eta \leq 1\}$.

3.1. *Fixed points*

The first step in unravelling the dynamics is to consider fixed points of our system. The trajectories, corresponding to solutions of the degenerate quartet with particular initial conditions, occupy the level curves of the Hamiltonian (2.16). We find that fixed points of (2.14) and (2.15) occur in four classes: $\eta = 0$ or 1 and $\theta = 0$ or $\pm\pi$. The upper and lower boundaries $\eta = 1$ and $\eta = 0$ correspond to a single wave train and a bichromatic wave train, respectively (recall $\eta = |B_a|^2/A$). These two well-known solutions of the Zakharov equation exhibit no energy exchange (see Leblanc 2009 or Mei *et al.* 2018, §§ 14.5 & 14.6), since $\mathrm{d}\eta/\mathrm{d}t = 0$ thereon. Indeed, the effect of nonlinear interaction in such cases is solely to induce a frequency correction, called Stokes' correction after Stokes (1847), and found for bichromatic waves by Longuet-Higgins & Phillips (1962); for a discussion in the context of the Zakharov equation, see Stuhlmeier & Stiassnie (2019).

Centre points at $\theta = 0$ and $\theta = \pm\pi$ correspond to steady-state near-resonant degenerate quartets of waves. Such solutions have been recently found using the homotopy analysis method (HAM) by Xu *et al.* (2012), Liao *et al.* (2016), Yang, Yang & Liu (2022) and others, for both resonant and near-resonant cases. The dynamics around such points is simple and can be described as time-dependent periodic exchanges of wave energy around the time-independent configuration, as noted by Xu *et al.* (2012). Exact analytical formulae for such periodic solution can also be obtained in terms of Jacobi elliptic functions, as done by Shemer & Stiassnie (1985).

To avoid overly bulky expressions, in what follows, we introduce the following notation:

$$\Delta' = \frac{\Delta}{AT_{aabc}}, \quad \Omega_0' = \frac{\Omega_0}{T_{aabc}} \quad \text{and} \quad \Omega_1' = \frac{\Omega_1}{T_{aabc}}. \tag{3.1a–c}$$

In these variables, we obtain fixed points at $\eta = 1$ of the form $(\theta, \eta) = (\theta_{\pm 1}, 1)$ whenever θ_1 satisfies

$$\cos(\theta_1) = \frac{\Delta' + \Omega_0' + \Omega_1'}{2}. \tag{3.2}$$

Such fixed points exist when the right-hand side is between -1 and 1, and $\theta_{-1} = -\theta_1$. These fixed points lie on the contour $H = -\Delta - A\Omega_0 - A\Omega_1/2$. Similarly, we obtain fixed points at $\eta = 0$ of the form $(\theta, \eta) = (\theta_{\pm 0}, 0)$ whenever θ_0 satisfies

$$\cos(\theta_0) = -\frac{\Delta' + \Omega_0'}{2}, \tag{3.3}$$

again provided the right-hand side is between -1 and 1 and $\theta_{-0} = -\theta_0$. These fixed points lie on the contour $H = 0$. Another class of fixed points is obtained for $\theta = 0$ or $\pm\pi$. In the former case, $(\theta, \eta) = (0, \eta_0)$ is a fixed point whenever

$$\eta_0 = \frac{2 + \Delta' + \Omega_0'}{4 - \Omega_1'}, \tag{3.4}$$

and $0 \leq \eta_0 \leq 1$. Note that $\eta_0 = 1$ if and only if $\theta_{\pm 1} = 0$, in which case, this fixed point coincides with (3.2). For $\theta = \pm\pi$, we find fixed points $(\pm\pi, \eta_\pi)$ provided

$$\eta_\pi = \frac{2 - (\Delta' + \Omega_0')}{4 + \Omega_1'}, \tag{3.5}$$

and $0 \leq \eta_\pi \leq 1$. Similarly, $\eta_\pi = 0$ if and only if $\theta_{\pm 0} = \pm\pi$, such that this fixed point coincides with (3.3).

3.2. *Phase portraits and bifurcation*

The dynamical system (2.14) and (2.15) contains two parameters – wave action A and mode-separation p – which together govern the existence of the fixed-points given in (3.2)–(3.5), and the attendant dynamics. The natural choice is to fix A – akin to specifying the total energy of waves – and to use mode separation as a bifurcation parameter.

In figure 1, we depict a series of characteristic phase portraits, where mode separation p increases from $p = 0$ in panel (*a*) to $p = 0.3$ in panel (*h*). In this figure, we have selected A equivalent to a carrier wave with steepness $\epsilon = 0.1$, so that $A = 2\pi^2/100$ (see (2.17) and recall $g = k_a = 1$). The figure thus represents both physically realistic, as well as characteristic behaviour, in a sense to be specified in detail below.

Deferring the details for the moment, we can give an overview of the dynamics of our degenerate quartet as obtained by phase-plane analysis, and shown in figure 1. In the limit of vanishing mode separation, figure 1(*a*), we find four fixed points: a centre at $\theta = 0$, a pair of saddle points on $\eta = 0$, located at $\theta = \pm 2\pi/3$, and a semi-stable fixed point at $\theta = \pm\pi$, $\eta = 1$. The first bifurcation occurs at $p = 0$, and as p increases, the semi-stable point at $(\theta, \eta) = (\pm\pi, 1)$ splits into three fixed points: a centre at $\theta = \pm\pi$ and two saddles at $\eta = 1$ (figure 1*b*). Further increase in the mode separation causes the centre at $\theta = \pm\pi$ to descend until the saddle connections between the two fixed points at $\eta = 0$ and $\eta = 1$

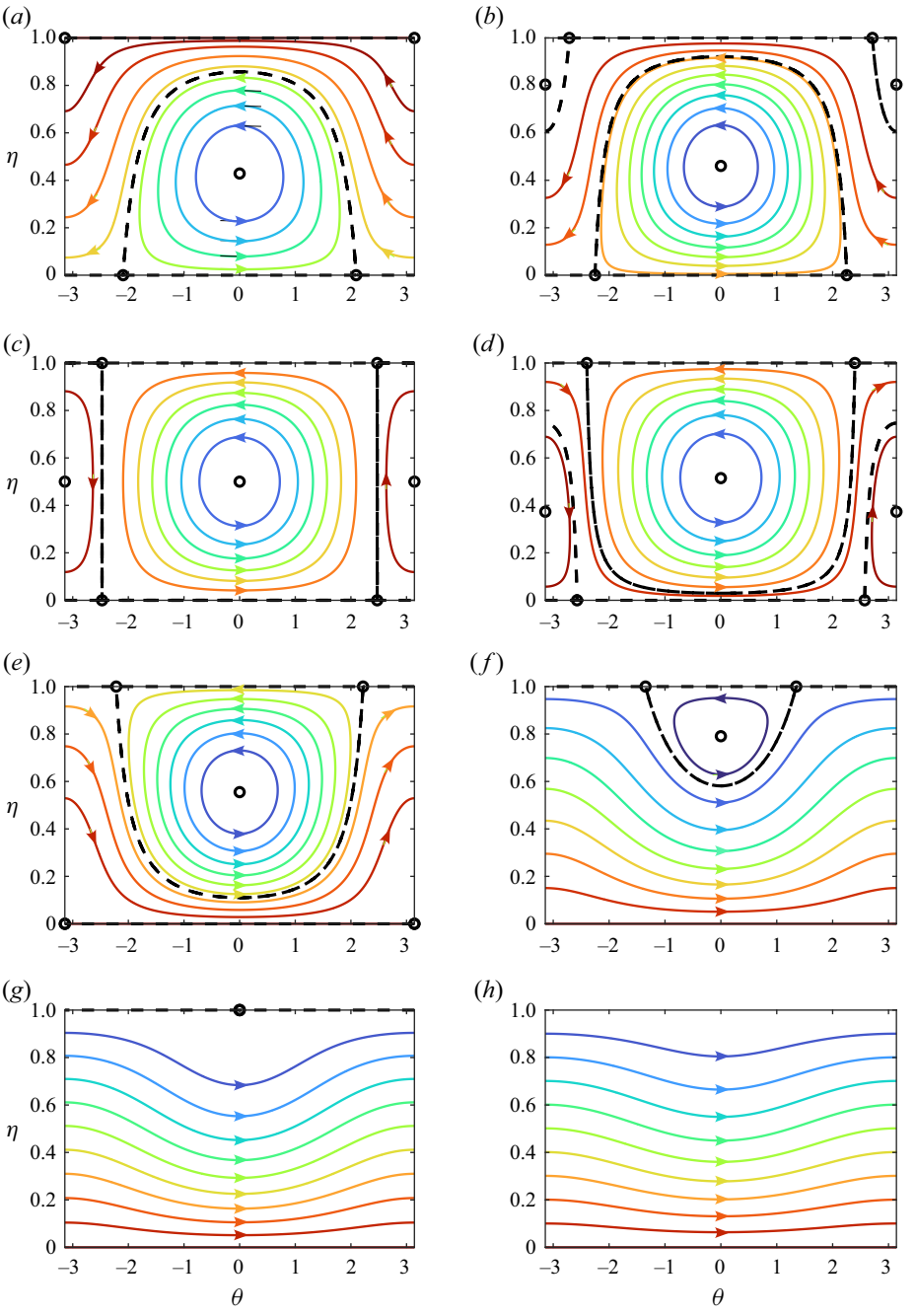

Figure 1. Phase portraits for $A = 2\pi^2/100$ and various values of mode separation p between 0 and 0.3, plotted on the cylinder $\{(\eta, \theta) \mid \eta \in [0, 1], \theta \in [-\pi, \pi]\}$. Coloured curves represent contours of the Hamiltonian (2.16). Dashed lines show separatrices, while dots denote fixed-points of the system. (*a*) $p = 0$, (*b*) $p = 0.06$, (*c*) $p = 0.0908771$, (*d*) $p = 0.1$, (*e*) $p = 0.120902$, (*f*) $p = 0.2$, (*g*) $p = 0.246206$ and (*h*) $p = 0.3$.

merge (figure 1*c*). This critical value of mode separation exhibits the maximal energy exchange among the interacting modes.

Further increasing p leads the centre at $\theta = \pm\pi$ to descend towards $\eta = 0$ (figure 1*d*) where it subsequently vanishes together with the saddle points along $\eta = 0$ (figure 1*e*). As the modes are separated further, the remaining three fixed points draw closer together in phase space (figure 1*f*) before coalescing (figure 1*g*) and disappearing entirely (figure 1*h*) – this last bifurcation leads to complete stabilisation of the system.

Separatrices (shown as dashed lines in figure 1) partition the phase plane. For example, in figure 1(*a*), we notice that interior solutions with initial values $\theta(0) < -2\pi/3$ or $\theta(0) > 2\pi/3$ are periodic and wind around the exterior of the separatrix connecting the pair of fixed points at $\eta = 0$. Such solutions take on all values of the phase from $-\pi$ to π. Other periodic solutions are confined to the interior of the separatrix, and wind around the centre at $\theta = 0$.

4. Nonlinear stability

While the phase-plane analysis presented above is remarkably simple, it contains a wealth of information about the fully nonlinear dynamics of interacting degenerate quartets of deep water waves. We focus first on a discussion of nonlinear instability results.

4.1. *Nonlinear instability of a uniform wave train*

Many classical studies of the stability of a uniform wave train begin by establishing that such a monochromatic wave is a solution of the relevant governing equation. This solution is then used as a starting point for linearisation and an instability criterion derived from the eigenvalues of the linear system, as done by Crawford *et al.* (1981). In our framework, uniform wave trains are described by $\eta = 1$, for arbitrary values of θ. The initial small disturbance used classically to investigate the Benjamin–Feir instability consists in imposing small sidebands, i.e. a shift to a contour $\eta < 1$. In figure 1(*a–f*), we readily observe that such a shift leads to growth of the sidebands, as η decreases along the contours, followed generically by periodic energy exchange. Maximal energy exchange occurs when η is changing fastest, and coincides with the smallest changes in the dynamic phase θ. Such phase coherence has also been observed in simulations, e.g. by Houtani, Sawada & Waseda (2022) and Liu, Waseda & Zhang (2021).

In fact, we can show that the classical linear stability criterion is equivalent to the existence of fixed points at $\eta = 1$ in the nonlinear system. The condition (3.2) for such fixed points to exist is

$$-1 \leq \frac{\Delta' + \Omega_0' + \Omega_1'}{2} \leq 1. \tag{4.1}$$

Squaring these inequalities, substituting Ω_0 and Ω_1 from (2.12) and (2.13), and using (2.17) yields, after simplification, the discriminant criterion

$$\left(\frac{\Delta}{2} + (T_a - T_{ab} - T_{ac})|B_a|^2\right)^2 - |B_a|^4 T_{aabc}^2 \leq 0, \tag{4.2}$$

see (Mei *et al.* 2018, (14.9.16)). It is rather surprising that this eigenvalue condition, which arises from an approach based on small amplitude perturbations (and which is oblivious to the existence of fixed-points of the original nonlinear problem), can be recovered exactly with our approach.

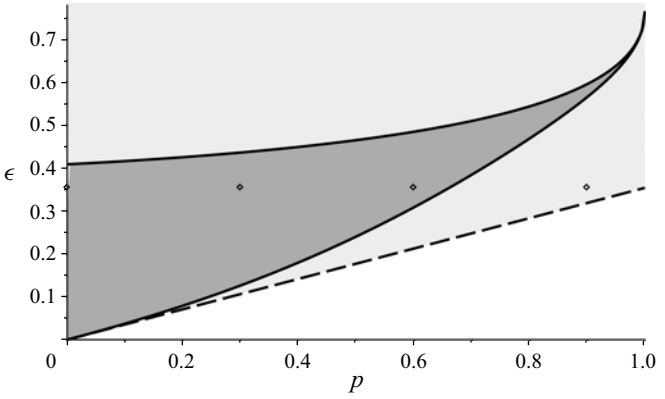

Figure 2. Existence of $\eta = 1$ fixed points in (ϵ, p)-parameter space according to (3.2). The dark shaded region denotes the nonlinear instability domain for the degenerate quartet. The dashed line denotes the lower boundary of the NLS instability threshold $\epsilon = p/\sqrt{8}$, which is shown in the light shaded region. For markers, refer to Appendix B.

4.1.1. *Stability boundaries and restabilisation*

The existence of fixed points at $\eta = 1$, and thus the instability of uniform wave trains to some perturbation, is the generic situation for degenerate quartets. We can appreciate this by considering (3.2), from which we establish that fixed points exist at $\eta = 1$ for some mode separation, provided $A \in [0, 2\pi(2-\sqrt{2})\sqrt{g}k_a^{-5/2}]$. Employing (2.17), this can be expressed in terms of carrier wave slope ϵ and implies the existence of fixed points (and thus instability) for

$$0 < \epsilon < \sqrt{2-\sqrt{2}}, \tag{4.3}$$

far beyond the wave breaking threshold.

In the limit of small mode separation, when the wavelengths of the sidebands are comparable to the carrier, we see that the instability domain remains bounded (see figure 2), with fixed points for $A \in [0, \sqrt{gk_a}\pi^2/3k_a]$. This yields the threshold

$$0 < \epsilon < \frac{1}{\sqrt{6}}, \tag{4.4}$$

which has previously been obtained numerically (see e.g. Yuen & Lake 1982, § VI.B.1). The simple, explicit formulae (4.3)–(4.4) presented here are the results of compact forms of the one-dimensional interaction kernels which allow for considerable algebraic simplification (see Appendix A and Kachulin *et al.* 2019).

In fact, this restabilisation for nearby sidebands (or long-wavelength disturbances) is a characteristic of the broadbanded Zakharov equation. Indeed, imposing a limit of narrow spectral bandwidth (in which the Zakharov equation reduces to the NLS) implies

$$\Omega_0' \to 1, \quad \Omega_1' \to -3 \quad \text{and} \quad \Delta' \to \frac{\omega_a p^2 \pi^2}{A k_a^5}. \tag{4.5a–c}$$

This can be used to reformulate the fixed-point criterion and recover the well-known instability threshold for NLS (Mei *et al.* 2018, (14.9.21)):

$$\frac{p}{k_a} \in [0, 2\sqrt{2}\epsilon]. \tag{4.6}$$

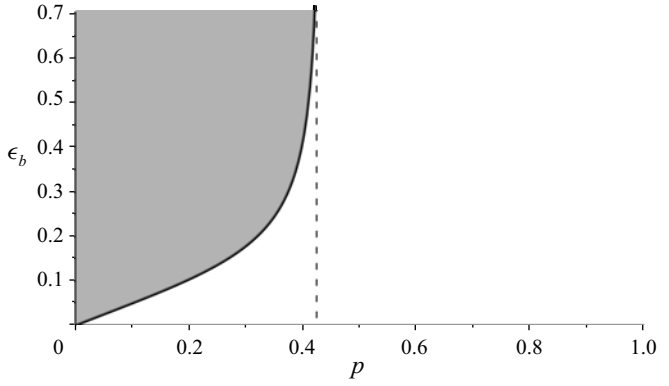

Figure 3. Existence of $\eta = 0$ fixed points in (ϵ_b, p)-parameter space, according to (3.3). The shaded region denotes the instability domain for a bichromatic wave train with equipartitioned mode amplitudes.

This is plotted in the (p, ϵ)-domain as the lightly shaded region above the dashed line $\epsilon = p/\sqrt{8}$ in figure 2. For small mode-separation distance p, the NLS instability criterion agrees well with the more general formulation of the Zakharov equation, as shown previously by Yuen & Lake (1982). However, the linear stability analysis of the NLS yields instability to perturbations with arbitrary separation provided the steepness ϵ is sufficiently large (see Appendix B for a comparison of the phase portraits).

For the truncated Zakharov equation, as mode-separation increases, larger values of carrier steepness ϵ are required to generate instability, up to the limit $p = 1$ when the instability domain contracts to the point $\epsilon = \sqrt{2 - \sqrt{2}}$. Conversely, for a given carrier steepness and increasing mode separation, the system will eventually exit the instability domain – this bifurcation is captured in figure 1(*g*), where fixed points at $\eta = 1$ coalesce and disappear.

4.2. *Nonlinear stability of a bichromatic wave train*

Instabilities of bichromatic wave trains, while less well-known than those for uniform wave trains, have also been studied, for example, by Leblanc (2009), Badulin *et al.* (1995) or Ioualalen & Kharif (1994). While our setting is somewhat different – in particular, we have only three unidirectional modes, in contrast to the four modes used by Leblanc 2009, § 4 to discuss class Ib instabilities – we can nevertheless obtain the nonlinear evolution of such instabilities by our phase-plane analysis, recalling that a bichromatic wave train occupies the line $\eta = 0$. In the present case, where the Fourier amplitudes of the sidebands k_b and k_c are taken to be identical, we naturally have a bichromatic wave train with waves of different steepness. Mode $k_b = (1 - p, 0)$ corresponds to a longer wave than mode $k_c = (1 + p, 0)$, and their slopes are related as

$$\epsilon_b^2 = \left(\frac{k_b}{k_c}\right)^{5/2} \epsilon_c^2, \tag{4.7}$$

see Mei *et al.* (2018, § 14.6). Without loss of generality, we depict the instability domain in terms of ϵ_b in figure 3.

The existence of fixed points – and consequent instability – of the bichromatic wave train is again seen to be generic. For any wave train, there exists a value of mode separation p such that the solution is unstable within the framework of the degenerate quartet.

This wave train stabilises for sufficiently large mode separation, as seen in the bifurcation in figure 1(*e*), when fixed points at $\eta = 0$ disappear. Moreover, we find a critical threshold for mode separation $p \approx 0.42$ beyond which bichromatic wave trains are stable.

5. Heteroclinic solutions

The existence of special solutions to the nonlinear Schrödinger equation (NLS) has attracted considerable attention in recent years, a discussion of which may be found in the work by Dysthe & Trulsen (1999) or, with an emphasis on hydrodynamics and experimental verification, by Chabchoub *et al.* (2014) and the references therein. We will see that several remarkable solutions – corresponding to heteroclinic orbits in the phase plane – exist for the three wave system. These include a discrete breather, i.e. a breather with finite spectral content, analogous to that found by Akhmediev, Eleonskiĭ & Kulagin (1987), Ablowitz & Herbst (1990), which approaches a plane wave as $t \to \pm\infty$. The form of the free surface and its envelope are of particular interest for such solutions; these can be recovered from the solution of the Zakharov equation (2.1) by defining the following complex amplitude function:

$$A(x,t) = \frac{1}{\pi}\left(\sqrt{\frac{\omega_a}{2g}}B_a\,\mathrm{e}^{\mathrm{i}(k_a x-\omega_a t)} + \sqrt{\frac{\omega_b}{2g}}B_b\,\mathrm{e}^{\mathrm{i}(k_b x-\omega_b t)} + \sqrt{\frac{\omega_c}{2g}}B_c\,\mathrm{e}^{\mathrm{i}(k_c x-\omega_c t)}\right). \tag{5.1}$$

The free surface elevation is then obtained as

$$\zeta(x,t) = \Re[A(x,t)], \tag{5.2}$$

and the envelope is $|A(x,t)|$.

5.1. *Discrete breather solutions*

The existence of special heteroclinic solutions, with properties similar to the well-known breather solutions of the nonlinear Schrödinger equation, clearly depends on the fixed points of our problem. Our approach is akin to that of Cappellini & Trillo (1991), who first investigated a three-mode truncation of the nonlinear Schrödinger equation.

5.1.1. *The discrete (1-1) Akhmediev breather*

For values of p and A satisfying (3.2) (see § 4.1 and figure 2), the two saddle points $(\theta, \eta) = (\pm\theta_1, 1)$ are connected by a heteroclinic orbit. Along this orbit, $\eta < 1$ and a trajectory approaches $(\pm\theta_1, 1)$ as $t \to \pm\infty$.

In fact, we can compute these solutions explicitly, by considering the following set of equations:

$$2\eta\cos(\theta) = \Delta' + \Omega_0' + \frac{\Omega_1'}{2}(1+\eta), \tag{5.3a}$$

$$\frac{\mathrm{d}\eta}{\mathrm{d}\theta} = \frac{\eta\sin(\theta)}{\cos(\theta) - \dfrac{\Omega_1'}{4}}, \tag{5.3b}$$

$$\frac{\mathrm{d}^2\theta}{\mathrm{d}t^2} = -2AT_{aabc}\sin(\theta)\frac{\mathrm{d}\theta}{\mathrm{d}t}. \tag{5.3c}$$

Equation (5.3*a*) follows from equating the Hamiltonian (2.16) to its value at $\eta = 1$. Equation (5.3*b*) is obtained from the implicit function theorem by regarding η as a function

of θ instead of t. Equation (5.3*c*) is obtained by taking the time derivative of (2.15). Equation (5.3*a*) is further used to simplify the form of (5.3*b*) and (5.3*c*).

Equation (5.3*b*) is separable and can be integrated directly to give

$$\eta = \frac{4\cos(\theta_1) - \Omega_1'}{4\cos(\theta) - \Omega_1'}, \tag{5.4}$$

where the integration constant is chosen so that the limits as θ tends to $\pm\theta_1$ are 1.

Equation (5.3*c*) can also be integrated to obtain

$$\frac{\mathrm{d}\theta}{\mathrm{d}t} = 2AT_{aabc}(\cos(\theta) - \cos(\theta_1)), \tag{5.5}$$

where the integration constant is chosen so that the limits as θ tends to $\pm\theta_1$ are 0. Integrating again yields an expression for the dynamic phase:

$$\tan(\theta/2) = \tan(\theta_1/2)\tanh(AT_{aabc}\sin(\theta_1)t), \tag{5.6}$$

where the integration constant was chosen so that $\theta(0) = 0$. Together, (5.6) and (5.4) describe the heteroclinic orbits shown in figure 1(*d–f*). (Note that the heteroclinic orbits around $\theta = \pm\pi$ in figure 1(*b*) can be treated similarly.)

The discrete (1-1) Akhmediev breather describes an orbit in phase space which connects one plane-wave solution with another. During the initial evolution, energy is transferred to the sidebands (η decreases) while the dynamic phase undergoes little change. Subsequent to this focusing, the energy-transfer process reverses, resulting in a phase-shifted plane wave. This situation is depicted in dimensionless coordinates in figure 4(*a*,*b*). Figure 4(*a*) shows the envelope, which is periodic in space and 'breathes' once at time $t = 0$, akin to the Akhmediev breather solution of the NLS. Figure 4(*b*) shows the free surface, which begins as a monochromatic plane wave, grows into a strongly modulated wave-train at $t = 0$ and reverts to a plane wave with an evident phase shift.

The discrete Akhmediev breather which occurs in the study of a single degenerate quartet is, in fact, the skeleton of the famed Akhmediev breather solution of the nonlinear Schrödinger equation; the latter likewise arises from the instability of a carrier wave and two equidistant sidebands, which subsequently induces a cascading instability as described by Chin, Ashour & Belić (2015). This makes a direct comparison possible, at least for the Fourier modes A_0 and A_1 of the Akhmediev breather (A_{-1} evolves analogously to A_1).

From Chin *et al.* (2015), we obtain the following exact equations for the Fourier modes of the Akhmediev breather:

$$A_0(t) = 1 - \frac{2(1-2a) + \mathrm{i}\lambda\tanh(\lambda t)}{\sqrt{1-\alpha^2}}, \tag{5.7}$$

$$A_1(t) = -\frac{2(1-2a) + \mathrm{i}\lambda\tanh(\lambda t)}{\sqrt{1-\alpha^2}}\left(\frac{1-\sqrt{1-\alpha^2}}{\alpha}\right). \tag{5.8}$$

The parameters a, α and λ can be related to our parameters p, ϵ_a as follows:

$$a = \frac{1 - (p/(2\sqrt{2}\epsilon_a))^2}{2}, \tag{5.9}$$

$$\lambda = \sqrt{8a(1-2a)}, \tag{5.10}$$

$$\alpha = \frac{\sqrt{2a}}{\cosh(\lambda t)}. \tag{5.11}$$

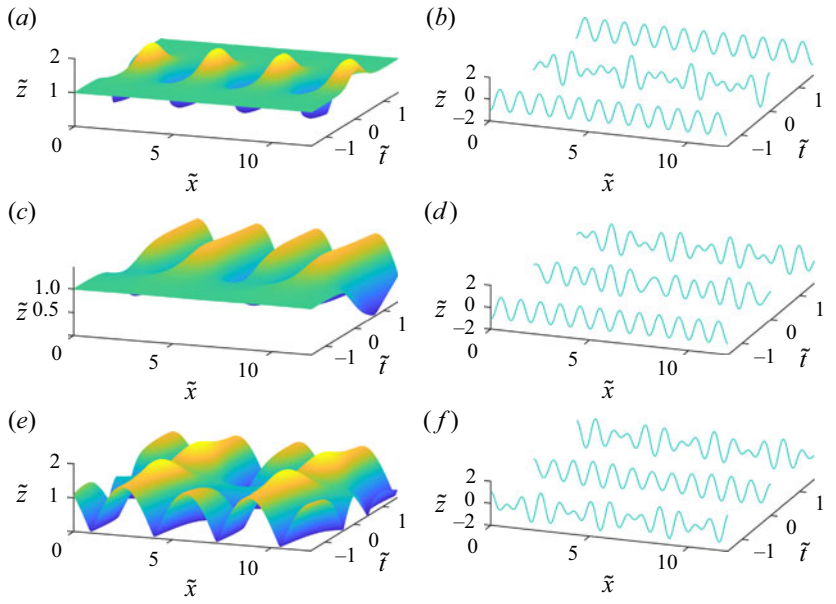

Figure 4. Time evolution of (*a*,*c*,*e*) the envelopes and (*b*,*d*,*f*) the free surface along different heteroclinic solutions. In all cases, the steepness of the wave k_a is set to $\epsilon_a = 0.2$. (*a*,*b*) Discrete Akhmediev breather for $p = 0.3012$; (*c*,*d*) (1-0) breather for the critical $p = 0.1670$; (*e*,*f*) (0-0) breather for $p = 0.1570$. Here, $\tilde{x} = xk_a/2\pi$, $\tilde{t} = t\omega_a/2\pi$ and $\tilde{z} = z/\epsilon_a$.

This ensures that we are comparing discrete and continuous Akhmediev breathers with the same spatial periodicity.

Figure 5 shows the time evolution of the carrier (blue curves) and one of the sidebands (red curves; recall that these evolve symmetrically) for the Akhmediev breather (dashed curves) and our discrete breather (solid curves). We take $\epsilon_a = 0.2$ with $p = 0.1$, 0.3 and 0.4 in each panel from top to bottom, respectively, and use the dimensionless time $\tilde{t} = AT_{aabc}t$.

There is qualitative resemblance and a degree of quantitative agreement in the evolution of the continuous breather and our three-mode model, particularly for intermediate mode separation and wave slope. However, as elucidated by Chin *et al.* (2015), the formation of the Akhmediev breather takes the form of an energy cascade wherein the energy of the carrier mode is distributed among all the infinite Fourier modes at $t = 0$. Since our model is truncated to three Fourier modes (the carrier wave and its sidebands only), this energy cascade is also truncated, leading to a surplus of energy remaining in the carrier wave simply because there are no more modes in the system. This is seen in figure 5 at $t = 0$, where the solid blue lines (modes $|B_a|$) sit above the dashed blue lines (modes $|A_0|$).

Figure 5(*c*) also illustrates the main difference between the Zakharov equation and the NLS for unidirectional waves, namely the difference in stability of a monochromatic wave train. The case $p = 0.4$ (figure 5*c*) is very close to the border of our stability region plotted in figure 2. Hence, the small energy exchange observed at $\tilde{t} = 0$. Once p is outside the instability region, there is no energy exchange (the phase portraits are akin to figure 1*h*) and no discrete breather solutions exist. The larger instability domain of the NLS, in contrast, continues to allow breather solutions, as reflected in the considerable energy exchange seen in figure 5(*c*) (dashed lines).

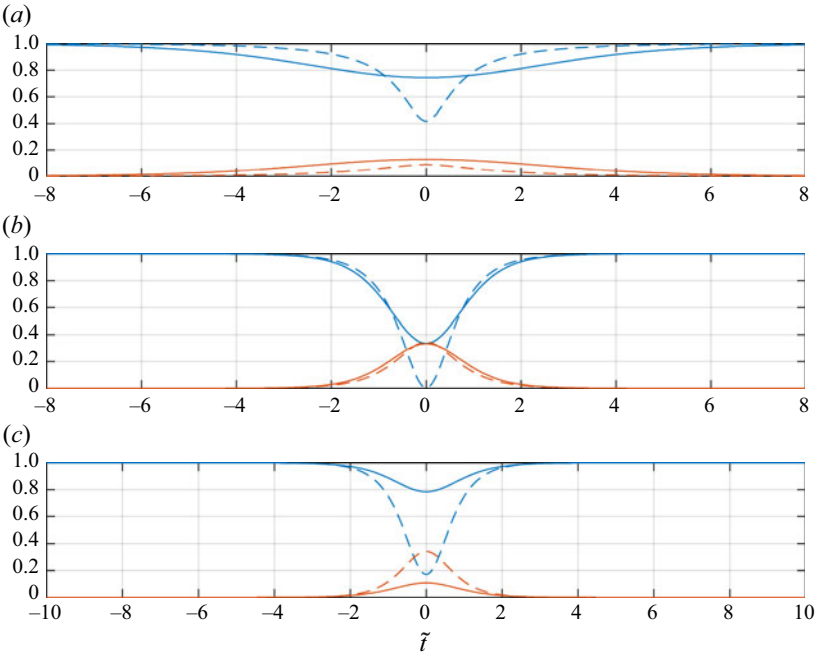

Figure 5. Comparison of the (1-1) discrete breather (solid lines) with the Akhmediev breather (dashed lines). Blue lines, time evolution of the carrier ($|B_a|^2$ and $|A_0|^2$, respectively). Red lines, time evolution of the sideband ($|B_b|^2$ and $|A_1|^2$, respectively). In all cases, $\epsilon_a = 0.2$. (*a*) $p = 0.1$. (*b*) $p = 0.3$. (*c*) $p = 0.4$.

5.1.2. *(1-0) breather and (0-1) breathers*

A special type of heteroclinic solution appears when the Hamiltonian at $\eta = 1$ vanishes, i.e. when p and A are such that $\Delta' + \Omega_0' + \Omega_1'/2 = 0$. There are two such heteroclinic solutions, one linking fixed points $(\theta_0, 0)$ and $(\theta_1, 1)$, and the other linking $(-\theta_1, 1)$ with $(-\theta_0, 0)$ (see figure 1*c*). These appear also in the context of optical fibres when the governing equation is the NLS, and are referred to as 'pump-depletion' solutions by Cappellini & Trillo (1991).

In this case, (2.14) simplifies to

$$\frac{\mathrm{d}\eta}{\mathrm{d}t} = \pm A T_{aabc}\eta(1-\eta)\sqrt{4 - \frac{\Omega_1'^2}{4}}, \tag{5.12}$$

where the sign depends on which fixed point we are considering. Integrating this equation yields

$$\eta = \frac{\mathrm{e}^{\pm A T_{aabc}\sqrt{4-\frac{\Omega_1'^2}{4}}\,t + C}}{\mathrm{e}^{\pm A T_{aabc}\sqrt{4-\frac{\Omega_1'^2}{4}}\,t + C} + 1}, \tag{5.13}$$

where C is an integration constant depending on the initial conditions. For instance, $C = 0$ for the initial condition $\eta(0) = \frac{1}{2}$. Assuming that a positive sign is chosen, the solution

tends to 1 as $t \to \infty$ and it tends to 0 as $t \to -\infty$. The limits are reversed if the negative sign is chosen.

The special case described by these orbits corresponds to a complete energy transfer from a uniform wave train to a bichromatic wave train (or *vice versa*), which appears hitherto not to have been observed in water waves. The envelope and free surface are depicted in figures 4(*c*) and 4(*d*), respectively. These show how spatially periodic modulation appears 'out of nowhere' with time t, or disappears as time is traversed in the negative sense.

5.1.3. *(0-0) breather*

For a given (sub-critical) value of mode separation p, and A such that (3.3) is satisfied (see 4.2 and figure 3), two distinct fixed points $(\theta, \eta) = (\pm\theta_0, 0)$ are linked by a heteroclinic solution that approaches $(\pm\theta_0, 0)$ as $t \to \mp\infty$, and along which $\eta > 0$. This solution satisfies the following set of equations:

$$2(\eta - 1)\cos(\theta) = \Delta' + \Omega_0' + \eta\frac{\Omega_1'}{2}, \tag{5.14a}$$

$$\frac{\mathrm{d}\eta}{\mathrm{d}\theta} = \frac{(1-\eta)\sin(\theta)}{\dfrac{\Omega_1'}{4} - \cos(\theta)}, \tag{5.14b}$$

$$\frac{\mathrm{d}^2\theta}{\mathrm{d}t^2} = 2AT_{aabc}\sin(\theta)\frac{\mathrm{d}\theta}{\mathrm{d}t}. \tag{5.14c}$$

As above, (5.14*a*) has been used to simplify (5.14*b*) and (5.14*c*).

Integrating (5.14*b*) yields

$$\eta = 2\frac{2\cos(\theta) + \Delta' + \Omega_0'}{4\cos(\theta) - \Omega_1'} = \frac{4\cos(\theta) - 4\cos(\theta_0)}{4\cos(\theta) - \Omega_1'}, \tag{5.15}$$

where the integration constant is chosen so that the limits as θ tends to θ_0 are 0.

Integrating (5.14*c*) yields

$$\frac{\mathrm{d}\theta}{\mathrm{d}t} = -2AT_{aabc}(\cos(\theta) - \cos(\theta_0)), \tag{5.16}$$

where the integration constant is chosen so the limits as θ tends to $\pm\theta_0$ are 0. Further integration yields

$$\tan(\theta/2) = -\tan(\theta_0/2)\tanh(\sin(\theta_0)AT_{aabc}t). \tag{5.17}$$

This solution is the natural counterpart to the discrete Akhmediev breather presented in § 5.1.1; however, rather than tending to a uniform wave train with $t \to \pm\infty$, it tends to a bichromatic wave train, again with an attendant phase shift. The envelope and free surface for such a case are shown in figures 4(*e*) and 4(*f*), respectively. At $t = 0$, the modulation is at a minimum, and the free surface elevation is close to a uniform wave train.

5.2. *Limiting solutions*

It is clear from (2.16) that the horizontal lines $\eta = 1$ and $\eta = 0$ are level lines of the Hamiltonian. Hence, any solution of (2.14) and (2.15) with suitable initial conditions so that $\eta = 1$ or $\eta = 0$ will remain on these lines.

As with the fixed points themselves, there is no energy exchange among the wave modes for these solutions. However, they are not steady (or stationary) solutions in the usual sense, because θ still satisfies the following differential equation:

$$\frac{\mathrm{d}\theta}{\mathrm{d}t} = \begin{cases} \Delta + A\Omega_0 + A\Omega_1 - 2AT_{aabc}\cos(\theta) & \text{for } \eta = 1, \\ \Delta + A\Omega_0 + 2AT_{aabc}\cos(\theta) & \text{for } \eta = 0. \end{cases} \tag{5.18}$$

A further differentiation of these equations with respect to t yields (5.3*c*) and (5.14*c*) respectively, which means that (5.6) and (5.17) are solutions for each case. Both limiting configurations of the system exhibit what is sometimes referred to as phase-locking or phase coherence; whereby, regardless of the initial phase, the dynamic phase converges to the fixed value $-\theta_1$ at $\eta = 1$ and θ_0 at $\eta = 0$. It is expected that if initial conditions are taken close to $\eta = 1$, i.e. if some small amount of energy is initially put in the sidebands, then a similar behaviour will be observed in the evolution of the combined phase, as has been recently reported by Houtani *et al.* (2022).

From the mathematical point of view, both limiting configurations $\eta = 1$ and $\eta = 0$ of the system can be understood as the limit of the generic periodic solutions, as all the energy goes to either the wave k_a, or is equipartitioned among the sidebands k_b and k_c, respectively. From a physical point of view, the dynamic phase θ disappears at both $\eta = 1$ or $\eta = 0$ configurations and one is left with a classical monochromatic Stokes waves or two co-propagating Stokes waves, respectively.

6. Discussion and conclusions

The reformulation of the discrete Zakharov equation for three modes as a two-dimensional Hamiltonian dynamical system provides a new and powerful perspective on a classical problem. In fact, the possibility of reformulating the Zakharov equations for a degenerate quartet in terms of only two auxiliary variables is intimately connected to the existence of an exact solution for this configuration, which can be given in terms of elliptic functions (see Shemer & Stiassnie 1985). With subsequent normalisations, it is possible to effectively describe the entire dynamics in terms of the total wave action A and a single bifurcation parameter p, the mode separation.

The mode separation governs the appearance of fixed points in the phase plane. Saddle points at $\eta = 1$ and $\eta = 0$ correspond to cases where the entire energy is concentrated in one or two Fourier modes, respectively; the centres correspond to a degenerate quartet of nearly resonant waves which undergoes no time evolution. These fixed points are simply another case of the steady-state waves recently discovered by Liao *et al.* (2016), Yang *et al.* (2022). Our phase-plane analysis provides a simple way to obtain these solutions, and highlights for the first time their critical role in organising the overall dynamics.

The existence of fixed-points on the boundaries $\eta = 1$ and $\eta = 0$ of our phase-space is intimately connected with the stability of uniform and bichromatic wave trains, respectively. When such fixed points are absent, the trajectories progress along nearly horizontal level lines on the cylindrical phase plane: the dynamic phase changes, but there is little redistribution of energy. Loosely speaking, we may say that the trajectories do not need to avoid the separatrices connecting the fixed points. The stability results we obtain for uniform wave trains demonstrate the robustness of the Benjamin–Feir condition, which we recover from the fully nonlinear system without any small-amplitude assumptions. For bichromatic wave trains, our setting appears to be different from those previously studied, and no comparable linear results appear to be available.

We also obtain numerous special solutions – including discrete breathers – which are identified with heteroclinic orbits in phase space. While the breather solutions of the nonlinear Schrödinger equation involve a continuum of modes, and therefore exhibit quantitatively different features, the two-dimensional phase space allows for an incisive and transparent analysis of these special solutions. It should be noted that, although breathers have sometimes been identified with homoclinic orbits, this terminology obscures the phase shift which is apparent in the *heteroclinic* connections between the saddle points.

The discrete breather solutions we obtain include an analogue of the Akhmediev breather, which arises from a plane-wave background, as well as limiting cases in which a uniform wave train becomes (as $t \to \infty$) a bichromatic wave train, and *vice versa*. While discrete Akhmediev breathers exist in large ranges of parameter space (and thus for many configurations of total energy and mode separation), the limiting (0,1) and (1,0) breathers are unique for given wave action A or mode separation p. In the context of water waves, we also find a seemingly new type of breather-like solution, which arises from, and returns to, a bichromatic background. The maximal energy exchange for this (0,0)-breather is therefore a 'demodulation', in which the envelope flattens out.

Breather-solutions of the continuous nonlinear Schrödinger equation have received considerable attention in recent years, both in fluid mechanics and optics (Mussot *et al.* 2018; Pierangeli *et al.* 2018; Vanderhaegen *et al.* 2021). While our new discrete breathers have some qualitative similarity with those obtained in the continuous model, there are notable quantitative differences. In particular, in our context, only three modes can be activated, so there is a limit to the cascading instability observed in the formation of the Akhmediev breather solution (Chin *et al.* 2015). This engenders differences in the breather's formation time, as well as in the maximum amplification. In a more general sense, the modulational instability of a single degenerate quartet – as considered in the present paper – captures many of the salient features of the Akhmediev breather, while significantly constraining the phase-space. Indeed, as more modes are considered, the dynamics can become chaotic (Annenkov & Shrira 2001), and the integrable three-mode theory we consider cannot capture the richness of possible behaviours.

Together with theoretical advances, there have been numerous recent experimental breakthroughs in the observation of breather solutions in water wave tanks (Chabchoub, Hoffmann & Akhmediev 2011; Chabchoub *et al.* 2012; Kimmoun *et al.* 2016; Gomel *et al.* 2021). In an experimental context, the waves evolve in space rather than time, and the evolution equations must be changed to reflect this: for unidirectional waves, the temporal Zakharov equation (2.1) can be replaced by an analogous spatial Zakharov equation, derived by Shemer *et al.* (2001), Shemer, Kit & Jiao (2002). The extent to which the new breathers agree with flume experiments poses an interesting question for future work.

Acknowledgements. We would like to thank the anonymous referees for numerous comments and suggestions which helped to improve the manuscript.

Funding. This work was supported by the Engineering & Physical Sciences Research Council (grant number EP/V012770/1).

Declaration of interests. The authors report no conflict of interest.

Author ORCIDs.
David Andrade https://orcid.org/0000-0002-9486-8200;
Raphael Stuhlmeier https://orcid.org/0000-0002-6568-1543.

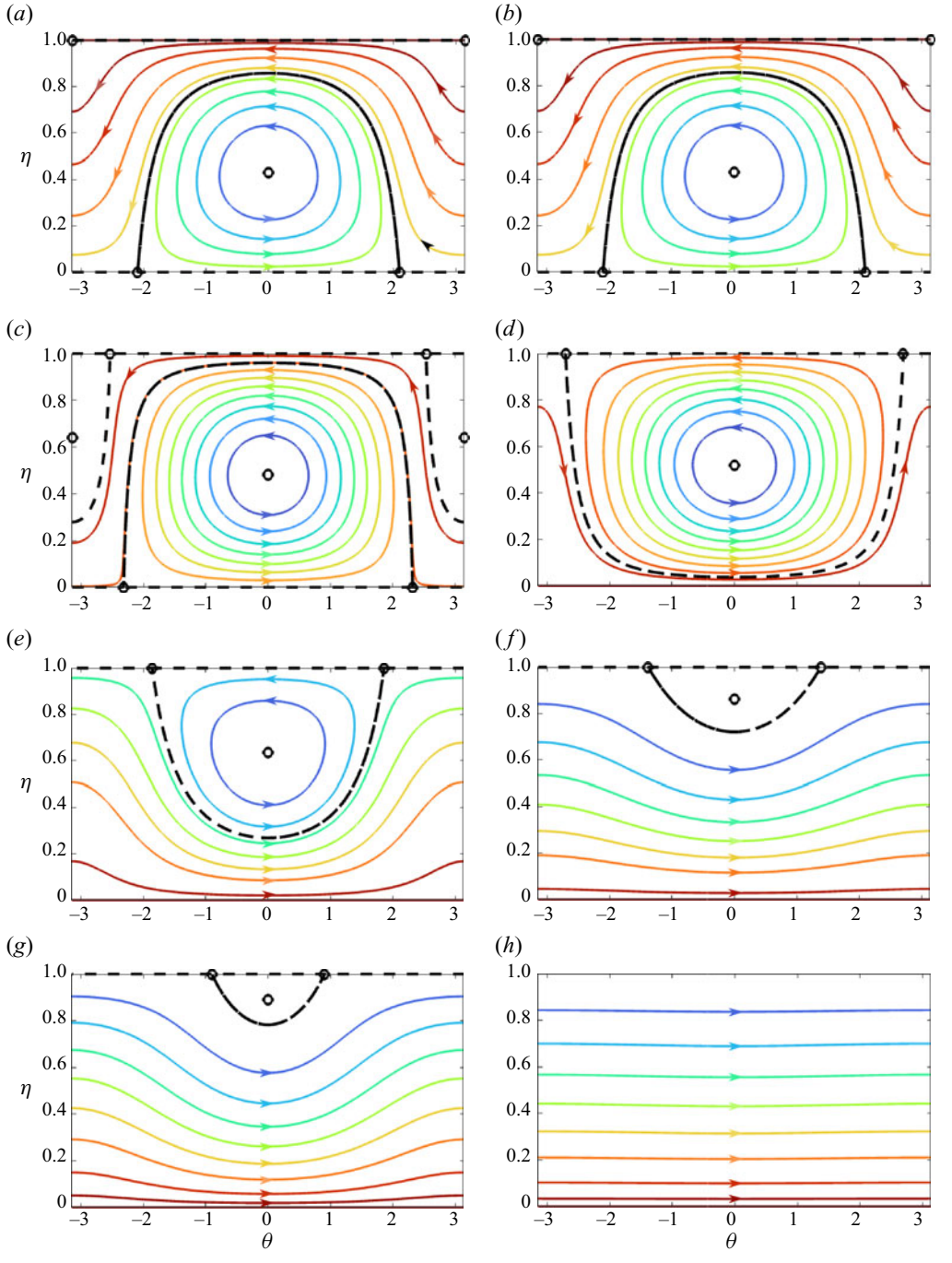

Figure 6. Phase portraits for $\epsilon = 1/\sqrt{8}$, mode separation $p = 0$ (*a*,*b*), 0.3 (*c*,*d*), 0.6 (*e*,*f*) and 0.9 (*g*,*h*) (see markers in figure 2) for the NLS (*a*,*c*,*e*,*g*) and Zakharov equation (*b*,*d*,*f*,*h*).

Appendix A. Interaction kernels

The interaction kernels appearing in the Zakharov equation (2.4) are lengthy, and expressions for these can be found in works by Mei *et al.* (2018) and Krasitskii (1994). For the case of unidirectional waves in deep water ($k_i > 0$ for all i) treated in the present study, considerable simplifications to the kernels are possible:

$$T(k,k,k,k) = \frac{k^3}{4\pi^2}, \tag{A1}$$

$$T(k_a,k_b,k_a,k_b) = \frac{1}{4\pi^2}k_a k_b \min(k_a,k_b), \tag{A2}$$

$$T(k_a,k_b,k_c,k_d) = \frac{(k_a k_b k_c k_d)^{1/4}}{32\pi^2}[(k_a k_b)^{1/2} + (k_c k_d)^{1/2}]$$
$$\times\,(k_a + k_b + k_c + k_d - [|k_a - k_c| + |k_a - k_d| + |k_b - k_c| + |k_b - k_d|]). \tag{A3}$$

The equation for T_{abcd} is taken from Kachulin *et al.* (2019) and adjusted by a factor of 2π. The kernels can be further simplified by making use of the homogeneity property $T(\alpha k_a, \alpha k_b, \alpha k_c, \alpha k_d) = \alpha^3 T(k_a,k_b,k_c,k_d)$. For a degenerate quartet of waves $2k_a = k_b + k_c$, this enables us to write the kernel

$$T(k_a,k_a,k_b,k_c) = \frac{1}{8\pi^2}[\min(k_b,k_c)(k_a^2 k_b k_c)^{1/4}(k_a + \sqrt{k_b k_c})]. \tag{A4}$$

Appendix B. Phase portraits for the nonlinear Schrödinger equation

Both qualitative and quantitative differences exist between the Zakharov formulation and its narrowband limit, the NLS. In particular, for $\epsilon > 1/\sqrt{8}$, the phase portraits of the NLS will always have fixed points at $\eta = 1$, since such waves are always unstable (see figures 2 and 6).

To emphasise this difference, in figure 6, we depict side-by-side phase portraits for a steepness of $\epsilon = 1/\sqrt{8}$. For vanishing mode separation $p = 0$ (figure 6*a*,*b*), the phase portraits coincide. However, as the mode separation increases, the NLS predicts that a monochromatic wave train is unstable to arbitrarily large perturbation wavenumbers (panels (*a*,*c*,*e*,*g*), which depict fixed points on $\eta = 1$ which persist up to $p = 1$). In contrast, the stability region of the Zakharov equation is bounded in (ϵ, p)-space, reflecting the more physically realistic situation in which waves of very different lengths do not exchange energy nor induce instability (panels (*b*,*d*,*f*,*h*).)

References

Ablowitz, M.J. & Herbst, B.M. 1990 On homoclinic structure and numerically induced chaos for the nonlinear Schrodinger equation. *SIAM J. Appl. Maths* **50** (2), 339–351.

Akhmediev, N.N., Eleonskiĭ, V.M. & Kulagin, N.E. 1987 First-order exact solutions of the nonlinear Schrödinger equation. *Teoret. Mat. Fiz.* **72** (2), 183–196.

Annenkov, S.Y. & Shrira, V.I. 2001 On the predictability of evolution of surface gravity and gravity-capillary waves. *Phys. D Nonlinear Phenom.* **152–153**, 665–675.

Badulin, S.I., Shrira, V.I., Kharif, C. & Ioualalen, M. 1995 On two approaches to the problem of instability of short-crested water waves. *J. Fluid Mech.* **303** (II), 297–326.

Benjamin, T.B. & Feir, J.E. 1967 The disintegration of wave trains on deep water. Part 1. Theory. *J. Fluid Mech.* **27** (03), 417–430.

Benney, D.J. 1962 Non-linear gravity wave interactions. *J. Fluid Mech.* **14**, 577–584.

Cappellini, G. & Trillo, S. 1991 Third-order three-wave mixing in single-mode fibers: exact solutions and spatial instability effects. *J. Opt. Soc. Am.* B **8** (4), 824–838.

CHABCHOUB, A., HOFFMANN, N. & AKHMEDIEV, N. 2011 Rogue wave observation in a water wave tank. *Phys. Rev. Lett.* **106** (20), 204502.

CHABCHOUB, A., HOFFMANN, N., ONORATO, M. & AKHMEDIEV, N. 2012 Super rogue waves: observation of a higher-order breather in water waves. *Phys. Rev.* X **2**, 011015.

CHABCHOUB, A., KIBLER, B., DUDLEY, J.M. & AKHMEDIEV, N. 2014 Hydrodynamics of periodic breathers. *Phil. Trans. R. Soc.* A *Math. Phys. Engng Sci.* **372**, 20140005.

CHIN, S.A., ASHOUR, O.A. & BELIĆ, M.R. 2015 Anatomy of the Akhmediev breather: cascading instability, first formation time, and Fermi-Pasta-Ulam recurrence. *Phys. Rev.* E - *Stat. Nonlinear Soft Matt. Phys.* **92** (6), 1–9.

CRAIK, A.D.D. 1986 *Wave Interactions and Fluid Flows*. Cambridge University Press.

CRAWFORD, D.R.R., LAKE, B.M.M., SAFFMAN, P.G.G. & YUEN, H.C.C. 1981 Stability of weakly nonlinear deep-water waves in two and three dimensions. *J. Fluid Mech.* **105**, 177–191.

DAVEY, A. & STEWARTSON, K. 1974 On three-dimensional packets of surface waves. *Proc. R. Soc.* A *Math. Phys. Engng Sci.* **338**, 101–110.

DYACHENKO, A.I., KACHULIN, D.I. & ZAKHAROV, V.E. 2017 Super compact equation for water waves. *J. Fluid Mech.* **828**, 661–679.

DYSTHE, K.B. 1979 Note on a modification to the nonlinear Schrodinger equation for application to deep water waves. *Proc. R. Soc.* A *Math. Phys. Engng Sci.* **369**, 105–114.

DYSTHE, K.B. & TRULSEN, K. 1999 Note on breather type solutions of the NLS as models for freak-waves. *Phys. Scr.* T **82**, 48–52.

GOMEL, A., CHABCHOUB, A., BRUNETTI, M., TRILLO, S., KASPARIAN, J. & ARMAROLI, A. 2021 Stabilization of unsteady nonlinear waves by phase-space manipulation. *Phys. Rev. Lett.* **126**, 174501.

GRAMSTAD, O. & TRULSEN, K. 2011 Hamiltonian form of the modified nonlinear Schrödinger equation for gravity waves on arbitrary depth. *J. Fluid Mech.* **670**, 404–426.

HASSELMANN, K. 1962 On the non-linear energy transfer in a gravity-wave spectrum. Part 1. General theory. *J. Fluid Mech.* **12** (04), 481–500.

HOUTANI, H., SAWADA, H. & WASEDA, T. 2022 Phase convergence and crest enhancement of modulated wave trains. *Fluids* **7** (8), 275.

IOUALALEN, M. & KHARIF, C. 1994 On the subharmonic instabilities of steady three-dimensional deep water waves. *J. Fluid Mech.* **262** (II), 265–291.

KACHULIN, D., DYACHENKO, A. & GELASH, A. 2019 Interactions of coherent structures on the surface of deep water. *Fluids* **4** (2), 1–21.

KIMMOUN, O., *et al.* 2016 Modulational instability and phase-shifted fermi-pasta-ulam recurrence. *Sci. Rep.* **6**, 1–9.

KRASITSKII, V.P. 1994 On reduced equations in the Hamiltonian theory of weakly nonlinear surface waves. *J. Fluid Mech.* **272**, 1–20.

LEBLANC, S. 2009 Stability of bichromatic gravity waves on deep water. *Eur. J. Mech. (*B*/Fluids)* **28** (5), 605–612.

LIAO, S., XU, D. & STIASSNIE, M. 2016 On the steady-state nearly resonant waves. *J. Fluid Mech.* **794**, 175–199.

LIU, S., WASEDA, T. & ZHANG, X. 2021 Phase locking phenomenon in the modulational instability of surface gravity waves. In *Proceedings of the 36th International Workshop on Water Waves and Floating Bodies (IWWWFB), Seoul, Korea*, pp. 25–28.

LONGUET-HIGGINS, M.S. & PHILLIPS, O.M. 1962 Phase velocity effects in tertiary wave interactions. *J. Fluid Mech.* **12** (03), 333–336.

MEI, C.C., STIASSNIE, M.A. & YUE, D.K.-P. 2018 *Theory and Applications of Ocean Surface Waves*, 3rd edn. World Scientific.

MUSSOT, A., NAVEAU, C., CONFORTI, M., KUDLINSKI, A., COPIE, F., SZRIFTGISER, P. & TRILLO, S. 2018 Fibre multi-wave mixing combs reveal the broken symmetry of Fermi–Pasta–Ulam recurrence. *Nat. Photonics* **12**, 303–308.

ONORATO, M. & SURET, P. 2016 Twenty years of progresses in oceanic rogue waves: the role played by weakly nonlinear models. *Nat. Hazards* **84** (2), 541–548. arXiv:1601.04317.

PHILLIPS, O.M. 1960 On the dynamics of unsteady gravity waves of finite amplitude. Part 1. The elementary interactions. *J. Fluid Mech.* **9** (2), 193–217.

PIERANGELI, D., FLAMMINI, M., ZHANG, L., MARCUCCI, G., AGRANAT, A.J., GRINEVICH, P.G., SANTINI, P.M., CONTI, C. & DELRE, E. 2018 Observation of Fermi-Pasta-Ulam-Tsingou recurrence and its exact dynamics. *Phys. Rev.* X **8** (4), 041017.

SHEMER, L., JIAO, H., KIT, E. & AGNON, Y. 2001 Evolution of a nonlinear wave field along a tank: experiments and numerical simulations based on the spatial Zakharov equation. *J. Fluid Mech.* **427**, 107–129.

SHEMER, L., KIT, E. & JIAO, H. 2002 An experimental and numerical study of the spatial evolution of unidirectional nonlinear water-wave groups. *Phys. Fluids* **14** (10), 3380–3390.

SHEMER, L. & STIASSNIE, M. 1985 Initial instability and long-time evolution of Stokes waves. In *The Ocean Surface: Wave Breaking, Turbulent Mixing and Radio Probing* (ed. Y. Toba & H. Mitsuyasu), pp. 51–57. D. Reidel.

SLUNYAEV, A.V. & SHRIRA, V.I. 2013 On the highest non-breaking wave in a group: fully nonlinear water wave breathers versus weakly nonlinear theory. *J. Fluid Mech.* **735**, 203–248.

STIASSNIE, M. 1984 Note on the modified nonlinear Schrödinger equation for deep water waves. *Wave Motion* **6** (4), 431–433.

STOKES, G.G. 1847 On the theory of oscillatory waves. *Trans. Camb. Phil. Soc.* **8**, 441–455.

STUHLMEIER, R. & STIASSNIE, M. 2019 Nonlinear dispersion for ocean surface waves. *J. Fluid Mech.* **859**, 49–58.

TRILLO, S. & WABNITZ, S. 1991 Dynamics of the nonlinear modulational instability in optical fibers. *Opt. Lett.* **16** (13), 986–988.

VANDERHAEGEN, G., NAVEAU, C., SZRIFTGISER, P., KUDLINSKI, A., CONFORTI, M., MUSSOT, A., ONORATO, M., TRILLO, S., CHABCHOUB, A. & AKHMEDIEV, N. 2021 "Extraordinary" modulation instability in optics and hydrodynamics. *Proc. Natl Acad. Sci.* **118** (14), e2019348118.

XU, D., LIN, Z., LIAO, S. & STIASSNIE, M. 2012 On the steady-state fully resonant progressive waves in water of finite depth. *J. Fluid Mech.* **710**, 379–418.

YANG, X., YANG, J. & LIU, Z. 2022 On the steady-state exactly resonant, nearly resonant, and non-resonant waves and their relationships. *Phys. Fluids* **34** (8), 082107.

YUEN, H.C. & LAKE, B.M. 1982 Nonlinear dynamics of deep-water gravity waves. In *Advances in Applied Mechanics*, pp. 68–229. Academic.

ZAKHAROV, V.E. 1968 Stability of periodic waves of finite amplitude on the surface of a deep fluid. *J. Appl. Mech. Tech. Phys.* **9** (2), 190–194.